Taylor & Francis
Taylor & Francis Group

Xenobiotica
the fate of foreign compounds in biological systems

ISSN: 0049-8254 (Print) 1366-5928 (Online) Journal homepage: www.tandfonline.com/journals/ixen20

Green synthesis of Zinc Oxide nanoflowers using *camellia sinensis* extract and evaluation of their xenobiotic-like cellular, apoptotic, and inflammatory responses in fibroblast cells

Serap Yesilkir Baydar

To cite this article: Serap Yesilkir Baydar (2026) Green synthesis of Zinc Oxide nanoflowers using *camellia sinensis* extract and evaluation of their xenobiotic-like cellular, apoptotic, and inflammatory responses in fibroblast cells, Xenobiotica, 56:1, 75-85, DOI: 10.1080/00498254.2025.2610230

To link to this article: https://doi.org/10.1080/00498254.2025.2610230

Published online: 04 Jan 2026.

Submit your article to this journal

Article views: 157

View related articles

View Crossmark data

Full Terms & Conditions of access and use can be found at
https://www.tandfonline.com/action/journalInformation?journalCode=ixen20

XENOBIOTICA
2026, VOL. 56, NO. 1, 75–85
https://doi.org/10.1080/00498254.2025.2610230

Taylor & Francis
Taylor & Francis Group

RESEARCH ARTICLE

Check for updates

Green synthesis of Zinc Oxide nanoflowers using *camellia sinensis* extract and evaluation of their xenobiotic-like cellular, apoptotic, and inflammatory responses in fibroblast cells

Serap Yesilkir Baydar[a,b]

[a]Department of Biomedical Engineering, Istanbul Gelisim University, Istanbul, Türkiye; [b]Life Sciences and Biomedical Engineering Application and Research Centre, Istanbul Gelisim University, Istanbul, Türkiye

ABSTRACT

1. Zinc oxide (ZnO) nanomaterials, acting as engineered xenobiotic-like agents, can induce complex cellular stress and defense responses. This study reports a novel green synthesis of ZnO nanoflowers using *Camellia sinensis* leaf extract, resulting in a biocompatible nanostructure with a distinctive flower-like morphology.
2. The *C. sinensis*-mediated synthesis provides a sustainable and reproducible approach for producing stable ZnO nanoflowers. The nanoparticles were thoroughly characterised (hydrodynamic assembly size: 259.3 nm; zeta potential: −32.35 mV; individual nanostructure physical dimensions: ~38.8×138.7 nm), and their biological interactions were evaluated in L929 fibroblasts to assess xenobiotic-like cellular responses.
3. Cytotoxicity was dose- and time-dependent (IC_{50} = 52.3 µg/mL at 24 h, 14.1 µg/mL at 48 h, and 10.5 µg/mL at 72 h). At a non-toxic IC_{50} concentration, the nanoflowers induced a transient adaptive stress response, characterised by significant yet reversible upregulation of inflammatory cytokines (IL-1β, IL-10) and key apoptotic regulators (Bax, Bcl-2, and p53).
4. Collectively, this study demonstrates that green-synthesised ZnO nanoflowers trigger moderate, self-resolving apoptotic and inflammatory signalling consistent with a xenobiotic-like adaptive cellular response. These findings highlight the potential of plant-mediated synthesis to engineer ZnO nanostructures with controlled bioactivity, supporting their safer application in biomedical contexts.

ARTICLE HISTORY
Received 13 October 2025
Revised 18 December 2025
Accepted 20 December 2025

KEYWORDS
Zinc Oxide nanoflowers; *Camellia sinensis*; green synthesis; xenobiotic-like response; cytotoxicity; nanotoxicology

Introduction

Zinc oxide nanoparticles (ZnO NPs) have garnered significant attention in xenobiotic and biomedical research due to their distinctive physicochemical properties, including a high surface area-to-volume ratio, pronounced photocatalytic activity, and notable biocompatibility. These features render ZnO NPs highly suitable for various biomedical applications such as targeted drug delivery, wound healing, biosensing, and cancer therapy (Jiang et al. 2018; Wiesmann et al. 2020; Hassan et al. 2021; Mahdi Ismail et al. 2023). From a xenobiotic perspective, the interaction of ZnO NPs with biological systems is complex, involving their absorption, distribution, metabolism, and excretion, as well as potential toxicological effects resulting from reactive oxygen species (ROS) generation and cellular responses to nanoparticle exposure.

Xenobiotic-like nanoparticles, which are engineered, upon entering a biological system, mimic the behaviour of classical xenobiotics. They undergo dynamic biological interactions in biological systems. Their physicochemical characteristics (e.g. size, surface charge, morphology, dissolution rate) directly influence these interactions, triggering cellular defence and stress pathways, including oxidative stress, inflammatory signalling, and programmed cell death. Evaluating nanoparticles through this xenobiotic perspective is crucial for predicting their biological fate, therapeutic efficacy, and long-term safety. Conventional synthesis of ZnO NPs typically employs chemical methods such as hydrothermal, solvothermal, sol-gel, and polyol-mediated techniques. These processes often require harsh conditions, including elevated temperatures (100 - 1000 °C), high pressures (up to 10,000 atm), and the use of toxic reagents like zinc acetate and sodium hydroxide, leading to considerable energy consumption and the generation of hazardous by-products. These factors contribute to environmental xenobiotic concerns due to chemical waste, potential bioaccumulation, and ecosystem toxicity if improperly managed (Mahamuni et al. 2019; Wu et al. 2019; Eric Kwabena et al. 2021; Hamed et al. 2023).

Moreover, standard chemical synthesis face challenges related to controlling nanoparticle size and morphology, frequently resulting in agglomeration that compromises particle uniformity and functional performance in biomedical contexts (Droepenu et al. 2022; Popa et al. 2023). Agglomerated ZnO NPs tend to exhibit altered biodistribution and cellular uptake profiles, influencing their xenobiotic behaviour and potential cytotoxicity (Droepenu et al. 2022). Although some methods can yield relatively uniform particles under controlled parameters, variability in temperature, pH, and

CONTACT Serap Yesilkir Baydar syesilkir@gelisim.edu.tr Department of Biomedical Engineering, Istanbul Gelisim University, Cihangir Dist. Sehit Jandarma Komando Er Hakan Oner Str. No:1 Avcilar, Istanbul, Türkiye
© 2026 Informa UK Limited, trading as Taylor & Francis Group

precursor ratios often disrupts reproducibility (Popa et al. 2023). Economically, these chemical synthesis incur high costs for raw materials, energy, and safety infrastructure, with scalability limited by technical and regulatory challenges tied to environmental xenobiotic management (Dhanya et al. 2014; Shalahuddin et al. 2019).

In response to these limitations, green synthesis approaches utilising biological entities such as plant extracts, bacteria, and fungi have emerged as eco-friendly alternatives, reducing reliance on toxic chemicals and harsh synthesis conditions (Narayana et al. 2020; Naiel et al. 2022; Murali et al. 2023; Hussien et al. 2025; Mahajan et al. 2025). Such biogenic methods often produce ZnO NPs with enhanced biocompatibility, lower environmental impact, and reduced xenobiotic risks (Narayana et al. 2020; Naiel et al. 2022; Hussien et al. 2025). Phytochemicals in plant extracts act as natural reducing and stabilising agents, enabling better control over nanoparticle size and shape, and yielding highly crystalline particles with diminished aggregation. These green-synthesised ZnO NPs have demonstrated promising antimicrobial, anticancer, and anti-inflammatory activities, aligning with safer xenobiotic profiles for therapeutic usage (Naiel et al. 2022; Hussien et al. 2025; Mahajan et al. 2025).

C. sinensis extract provides a rapid, reproducible, and environmentally sustainable route to ZnO NP synthesis, leveraging its high content of polyphenols, flavonoids, and antioxidants as reducing and capping agents. This results in stable, crystalline ZnO nanostructures with controlled size (typically 26–168 nm) and morphology, minimising agglomeration and optimising their physicochemical and biological properties (Baskaran and Subash 2021; Kumar et al. 2023; Benaiche et al. 2025). The simple, cost-effective, and scalable nature of *C. sinensis*-mediated synthesis supports broader industrial and biomedical applications, while aligning with principles of green chemistry and xenobiotic reduction.

Despite existing work on *C. sinensis*-based ZnO NP biosynthesis, most studies focus on synthesis and basic characterisation, with limited exploration of nanoparticle morphology control and the associated xenobiotic implications (Bibi et al. 2017; Ali et al. 2022). The abundant biomolecules in *C. sinensis* extract (polyphenols, flavonoids, catechins, tannins) facilitate metal ion reduction by electron donation, promoting nucleation and growth while capping the particle surface to prevent excess aggregation. This regulation is crucial for controlling size, shape, and ultimately nanomaterial interaction with biological systems and xenobiotic fate. Specifically, ZnO nanoflowers possess a unique three-dimensional morphology with a large surface area that enhances their biological activities and modulates toxicity profiles favourably.

This study presents a sustainable, plant-mediated method for synthesising ZnO nanoflowers as engineered xenobiotic-like agents. The research aims to thoroughly characterize their physicochemical properties and evaluate biosafety by assessing cellular inflammatory and apoptotic responses through *in vitro* cytotoxicity and functional assays. Such foundational analysis contributes to understanding the xenobiotic behaviour of these nanomaterials, facilitating safer design and application in biomedical fields, and addressing environmental and health safety challenges inherent in nanoparticle use.

Materials and methods

Chemicals and reagents

Reagents for nanoparticle synthesis. Zinc nitrate hexahydrate [$Zn(NO_3)_2{\cdot}6H_2O$, ≥99% purity, MW: 297.48 g/mol], potassium hydroxide (KOH, MW: 56.11 g/mol), and ethanol (≥99.5% purity) were purchased from Sigma-Aldrich (USA) used for washing and purification steps. All reagents employed in the synthesis were of analytical grade. Deionised water was consistently used throughout the experimental process. *C. sinensis* leaves were procured from a local vendor in Istanbul, Türkiye.

Reagents for cell culture. The L929 murine fibroblast cell line was acquired from the American Type Culture Collection (ATCC, Manassas, USA). Dulbecco's Modified Eagle Medium/Nutrient Mixture F-12 (DMEM-F12) was sourced from Pan Biotech (Germany). Foetal bovine serum (FBS), along with penicillin, streptomycin, and trypsin-EDTA, were procured from Sigma-Aldrich/Merck (USA). Additional chemicals used in cytotoxicity and functional assays, including ethanol and Folin reagent, were sourced from CAPP (Denmark), Neofroxx/BioFroxx (Germany), and Sigma-Aldrich/Merck (USA).

Preparation of Camellia sinensis extract. Dried leaves of *C. sinensis* were pulverised into a fine powder using a laboratory grinder and stored in sealed, light-resistant containers at room temperature until extraction. Aqueous extract was freshly prepared by mixing 20 g of fine powder of *C. sinensis* with 200 mL distilled water and then soaking it in a water bath at 50 °C for 6 h (Baydar et al. 2025). Then it was filtered using Whatman No. 42 filter paper and centrifuged for 10 min at 6000 rpm. Finally, the supernatant was decanted (Senthilkumar and Thirumal 2014) and the residual materials were stored at −20 °C in sealed amber vials until further applications.

Green synthesis of Zinc Oxide nanoparticles. The synthesis was performed according to a previously optimised and published protocol (Baydar et al. 2025). Briefly, 100 mL of a 0.2 N $Zn(NO_3)_2{\cdot}6H_2O$ aqueous solution was prepared. One hundred millilitres (100 mL) of C. sinensis leaf extract, prepared at a concentration of 50 mg of dried extract solids per mL of distilled water (equivalent to a total of 5.0 g of extract solids), supplemented with Dimethyl Sulfoxide (DMSO) ≤ 0.1% v/v, was added dropwise to the zinc nitrate solution under continuous magnetic stirring at 600 rpm, while maintaining the temperature at 70 °C. The reaction was visually monitored till a distinct colour change from brownish to yellowish indicated the formation of Zinc Oxide precursors. Subsequently, a 0.4 N KOH solution was added dropwise until the pH reached 12. The resulting mixture was stirred for an additional 45 min. The resulting whitish precipitate was harvested by centrifugation at 12,000 rpm for 10 min, followed by two successive washes with distilled water and ethanol. The collected material was then pre-dried in an oven at 60 °C for 2 h. Subsequently, the dried powder underwent calcination in a muffle furnace at 500 °C for 3 h. The synthesis process of ZnO NPs is depicted in Figure 1.

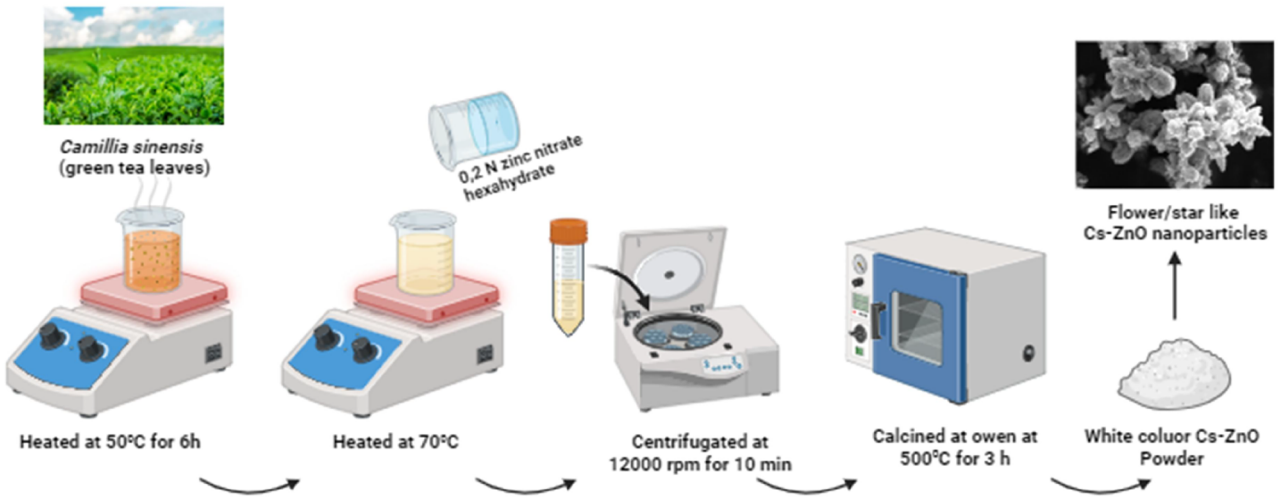


Figure 1. Schematic illustration of the synthesis procedure of ZnO NPs (Created in BioRender.com).

Preparation and sterilisation of nanoparticle suspensions for cell treatment. For the *in vitro* assays, the stock suspension of biosynthesized ZnO nanoflowers was prepared by dispersing the powdered sample in sterile, endotoxin-free deionised water and subjecting it to sonication for 30 min to ensure a homogenous dispersion. Subsequently, this suspension was transferred to an open sterile Petri dish within a laminar flow hood and exposed to germicidal UV-C light (254 nm wavelength) for 60 min with periodic gentle swirling to ensure uniform exposure. This duration is based on established protocols sufficient to inactivate microbial contaminants (Lee et al. 2008). Following UV sterilisation, the suspension was used immediately to prepare the serial dilutions in complete cell culture medium for treatment.

Characterisation of Zinc Oxide nanoparticles. To comprehensively evaluate the physicochemical properties of the green-synthesised ZnO NPs, which elucidate critical parameters, including particle size distribution, surface charge, stability, optical behaviour, and morphological features, a series of advanced analytical techniques, including dynamic light scattering and zeta potential measurements, UV-visible spectroscopy (Shimadzu, UV–Vis 1800, Japan). for optical analysis, and high-resolution imaging *via* field emission scanning electron microscopy (FESEM - (Apreo 2S, Thermo Scientific, USA) were employed.

Dynamic light scattering and zeta potential analysis. The particle size distribution, polydispersity index (PDI), and zeta potential of the green-synthesised ZnO NPs were determined using the SZ-100 nanoparticle analyser (Horiba Scientific, Japan) (Baydar et al. 2025). For analysis, 0.1 mg of ZnO NP powder was dispersed in 10 mL of deionised water and sonicated to ensure uniform suspension. The hydrodynamic diameter and size distribution of biosynthesized ZnO NPs were characterised at a fixed scattering angle of 90° and a controlled temperature of 25 °C. Zeta potential measurements were conducted to evaluate the surface charge and colloidal stability of the biosynthesized ZnO NPs.

Optical characterisation. The optical properties of the ZnO NPs were assessed using a UV-visible spectrophotometer. The NPs were dispersed in distilled water, and the absorbance spectrum was recorded over the 200–600 nm wavelength range.

Nano-structural imaging. The synthesised ZnO NPs' surface morphology and structural characteristics were examined using a FESEM operated at accelerating voltages between 1 and 5 kV. Samples were prepared by placing a small amount of the NP powder onto carbon-coated adhesive tapes mounted on aluminium stubs, followed by sputter-coating with a thin layer of gold to enhance conductivity.

Fourier-transform infra-red spectroscopy. Fourier-transform infra-red spectroscopy (FTIR) was employed to identify the functional groups present on the surface of the biosynthesized ZnO nanoparticles and to confirm the involvement of *C. sinensis* phytochemicals in nanoparticle capping. The analysis was performed using an FTIR spectrometer (Bruker, Vertex 70 ATR, USA). A small quantity of the dried ZnO nanoparticle powder was thoroughly mixed with spectroscopically pure potassium bromide (KBr) at an approximate ratio of 1:100 and pressed into a transparent pellet using a hydraulic press. Background scans were collected using a pure KBr pellet. Spectra were recorded in transmission mode across the mid-infra-red range of 4000 to 400 cm^{-1} with a resolution of 4 cm^{-1} and an accumulation of 32 scans per spectrum to ensure an adequate signal-to-noise ratio. The obtained spectra were baseline-corrected and analysed to identify characteristic vibrational bands corresponding to metal-oxygen bonds and organic functional groups.

In vitro biosafety evaluation

Cell line and culture conditions. The L929 mouse skin fibroblasts, as stipulated by ISO standards for the biological assessment of biomaterials intended for medical use (Słota et al. 2021) were cultured in DMEM-F12 enriched with 10% fetal bovine serum (FBS), 100 U/mL penicillin, and 100 µg/mL streptomycin (PEST). The cells were maintained in a humidified incubator at 37 °C with 5% CO_2. Once the cultures reached approximately 80% confluency, the cells were detached using a trypsin-EDTA solution and subsequently counted using a haemocytometer (Marienfeld, Germany). They were then seeded at the required density into T25 culture flasks and kept under identical incubation conditions until further use

in experimental assays (Karamanlioglu and Yesilkir-Baydar 2022).

Real-time cytotoxicity assessment. The cytotoxic effects of green-synthesised ZnO NPs were evaluated using the xCELLigence real-time cell analysis (RTCA) system (Agilent Technologies, Santa Clara, CA, USA), which monitors cell viability and proliferation by measuring electrical impedance across microelectrodes integrated into the bottom of specialised e-plates. This label-free, impedance-based method allows for continuous, real-time monitoring of cellular events, including adhesion, spreading, and proliferation (Ibrahim et al. 2021)

For the assay, L929 cells were seeded into 96-well E-plates at a density of 2×10^4 cells/mL and allowed to adhere and proliferate for 24 h under standard culture conditions. After this incubation period, the cells were treated with varying concentrations of ZnO NPs (2.5, 5, 10, 25, 50, 100, and 250 µg/mL) and incubated for 24, 48, and 72 h, while untreated wells served as controls. Impedance was recorded every 15 min and expressed as the Cell Index (CI). The normalised cell index (NCI) was calculated as $NCI = CI_t/CI_baseline$, with CI_baseline defined as the time point immediately before nanoparticle exposure. This normalisation allowed accurate comparison of cell responses across time and concentrations.

IC_{50} values for 24, 48, and 72 h were calculated from the NCI data. Analysis was performed using RTCA Software Pro (Agilent Technologies), which applies a sigmoidal dose–response model based on a four-parameter logistic (4PL) fit (Top, Bottom, $logIC_{50}$, Hill slope) to determine the half-maximal inhibitory concentrations (Limame et al. 2012; Atmaca et al. 2016).

Functional bioactivity assays

Cellular inflammatory response assay. The expression levels of key inflammatory cytokines, interleukin-1 beta (IL-1β) and interleukin-10 (IL-10), were quantified at 24-, 48-, and 72-hours post-treatment with the non-toxic concentration IC_5 of biosynthesized ZnO NPs using enzyme-linked immunosorbent assay (ELISA). Measurements were conducted using a microplate reader (Multiskan GO, Thermo Scientific, USA). The assays were carried out following the manufacturer's instructions with commercially available, mouse-specific ELISA kits (SunRedBio Technology Co., Ltd., Shanghai, China). All procedures adhered to standardised protocols to ensure the reliability and reproducibility of the cytokine quantification.

Apoptotic response assay. Total RNA was isolated from L929 cells at 24-, 48-, and 72-hours post-treatment with the non-toxic concentration IC_{50} of biosynthesized ZnO NPs using the RNeasy Protect Mini Kit (Qiagen, Germany). RNA concentration and purity were determined using a NanoDrop™ spectrophotometer (Thermo Fisher Scientific, USA), evaluating absorbance ratios at 260/280 nm and 260/230 nm. Samples with A260/280 ratios between 1.8 and 2.0 and A260/230 ratios above 2.0 were considered acceptable for downstream applications. Complementary DNA (cDNA) was synthesised from the extracted RNA using a commercially available reverse transcription kit (A.B.T. Lab Industry, Türkiye). Quantitative real-time PCR (qPCR) using a SYBR Green-based 2× qPCR MasterMix (A.B.T. Lab Industry, Türkiye) on a StepOnePlus Real-Time PCR System (Applied Biosystems, Germany) was employed to assess the relative expression levels of key apoptosis-related genes by melting curve analysis using respective primers (Table 1) targeting Bax, Bcl-2, and p53 in L929 cells. GAPDH was used as the internal reference gene for normalisation. Untreated samples for each target gene (p53, BCL-2, BAX, and GAPDH) were used as baseline controls, serving as reference points for evaluating gene expression changes in the treated groups. All reactions were performed in triplicate to ensure reproducibility, and no-template controls (NTCs) were included as technical negative controls to monitor potential contamination or non-specific amplification. Ct values greater than 40 were excluded from the analysis. Relative gene expression was calculated using the $2^{\Delta\Delta Ct}$ method.

Table 1. Primer sequence used for apoptotic response assay.

Gene ID		Sequences (5′ -> 3′)
Bcl-2	F	CCT GTG CAC CAA GGT GCC GGA ACT
	R	CCA CCC TGG TCT TGG ATC CAG CC
Bax	F	TGC AGA GGA TGA TTG CCG CCG
	R	ACC CAA CCA CCC TGG TGT TGG
p53	F	GCC CAA CAA CAC CAG CTC CT
	R	CCT GGG CAT CCT TGA GTT CC
GAPDH	F	AGG GCA AGA TGG CTG TAA GGT
	R	GGG ACC AAC TTC GGA ATC AG

Statistical analysis. Quantitative values from repeated measurements of DLS analysis and zeta potential are presented as mean ± standard deviation (SD). The fold change in CI values of *C. sinensis* mediated-ZnO NP-treated cells was calculated relative to the untreated control group at 24 h, 48 h, and 72 h. Expression levels of IL-1β and IL-10 cytokines, as well as the regulation of apoptotic genes Bax, Bcl-2, and p53, are reported as mean ± standard deviation based on three independent replicates per group.

Statistical comparisons among treatment groups (Control, 24, 48, and 72 h) were performed separately for each gene using one-way ANOVA followed by Tukey's post hoc test. Effect sizes were estimated using eta squared (η^2). All analyses were conducted in R version 4.3.2 (R Foundation, Vienna, Austria). A 95% confidence interval was applied, and statistical significance was defined as $p < 0.05$.

Results

Morphological characterisation of biofabricated Zinc Oxide nanoparticles

ZnO NPs synthesised using *C. sinensis* extract were obtained as a yellowish-white powder. Field emission scanning electron microscopy (FESEM) imaging of the biofabricated ZnO NPs, performed at x100,000 and x200,000 magnification, revealed a distinctive flower-like morphology with individual nanostructure physical dimensions, expressed as mean values derived from multiple randomly selected measurements, were approximately 38.8 × 138.7 nm (Figure 2).

Dynamic light scattering (DLS) analysis and zeta potential

The DLS results revealed hydrodynamic nonoflower assembly size mean of 259.3 nm, with a SD of 26.0 nm and a mode size of 261.0 nm (Figure 3a). The total scattering intensity count rate was recorded at 2982 kCPS, and the sample transmission

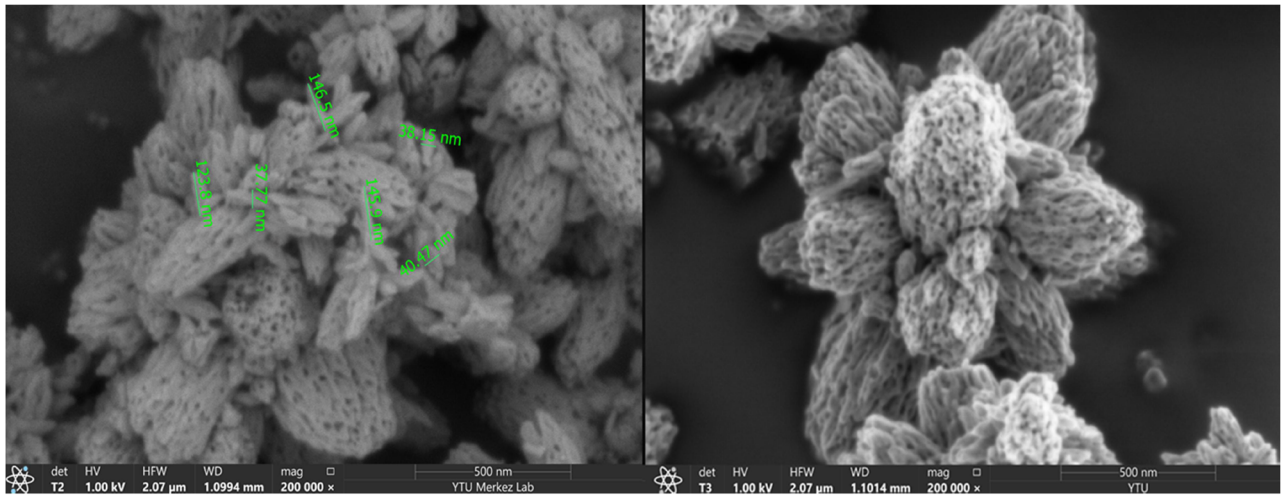


Figure 2. FESEM images of flower-like ZnO NPs a) x100.000 and b) x200.000 magnification.

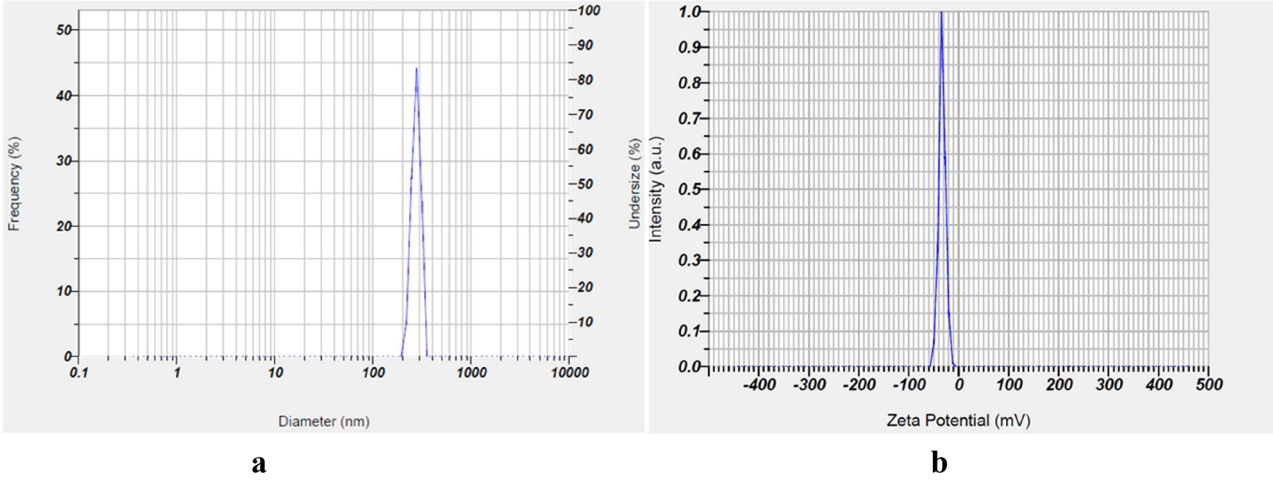


Figure 3. Dynamic light scattering (a) and zeta potential (b) analysis of *C. sinensis*-mediated ZnO NPs. (a) Size distribution histogram showing a mean hydrodynamic diameter of 259.3 nm. (b) Zeta potential distribution with an average value of −32.35 ± 0.78 mV, indicating high colloidal stability.

before measurement was 25,515, confirming adequate sample clarity and measurement quality. These results show a uniform nanoparticle population with limited polydispersity.

The average zeta potential of the biosynthesized ZnO NPs was measured as −32.35 ± 0.78 mV (Figure 3b). The corresponding electrophoretic mobility was −0.0002505 ± 0.000006 $cm^2/V{\cdot}s$.

UV–visible spectroscopy analysis

A distinct, clear and unimodal absorption peak was observed at approximately 330 nm (Figure 4), which is characteristic of the intrinsic band-gap absorption of ZnO NPs. This absorption profile confirms the successful synthesis of ZnO NPs and is consistent with previously reported spectra for biosynthesized ZnO nanostructures.

Fourier-Transform infrared (FTIR) spectroscopy

The FTIR spectroscopy illustrates the spectrum of dried ZnO nanoparticles recorded between 400 and 4000 cm^{-1}. The stretching vibrations of the Zn–O bond give rise to absorption bands at approximately 450 cm^{-1}, 556 cm^{-1}, 656 cm^{-1}, and 903 cm^{-1}. Additionally, bands observed near 1521 and 1381 cm^{-1} correspond to the asymmetric and symmetric stretching modes of zinc-associated carboxylate (C=O) groups (Figure 5).

Cytotoxicity and monitoring cell proliferation

The cytotoxic effects of ZnO NPs were assessed across a range of concentrations (2.5, 5, 10, 25, 50, 100, and 250 µg/mL) using the xCELLigence system. Real-time impedance analysis revealed a clear dose- and time-dependent cytotoxic response of L929 cells following exposure to ZnO NPs (Figure 6). Both the cell index (CI) and normalised cell index (NCI) curves showed an immediate decline after nanoparticle addition, indicating rapid onset of cytotoxicity. Sigmoidal dose–response modelling demonstrated progressive increases in sensitivity over time, with the calculated IC_{50} values decreasing from 52.3 µg/mL at 24 h to 14.1 µg/mL at 48 h and 10.5 µg/

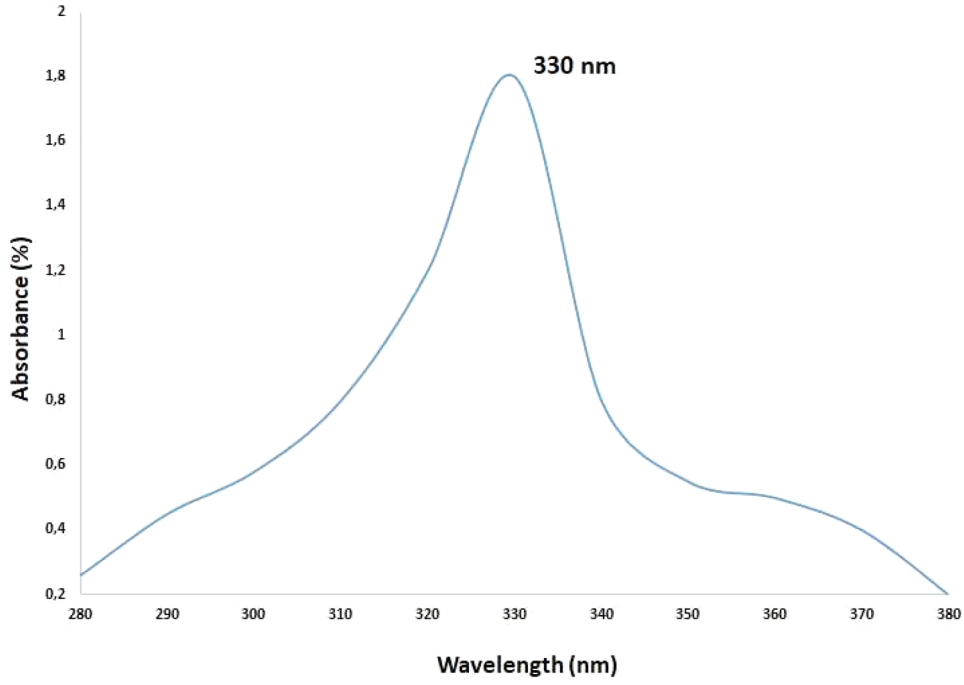


Figure 4. UV–Visible absorption spectrum of *C. sinensis*-mediated ZnO NPs showing a characteristic peak at 330 nm.

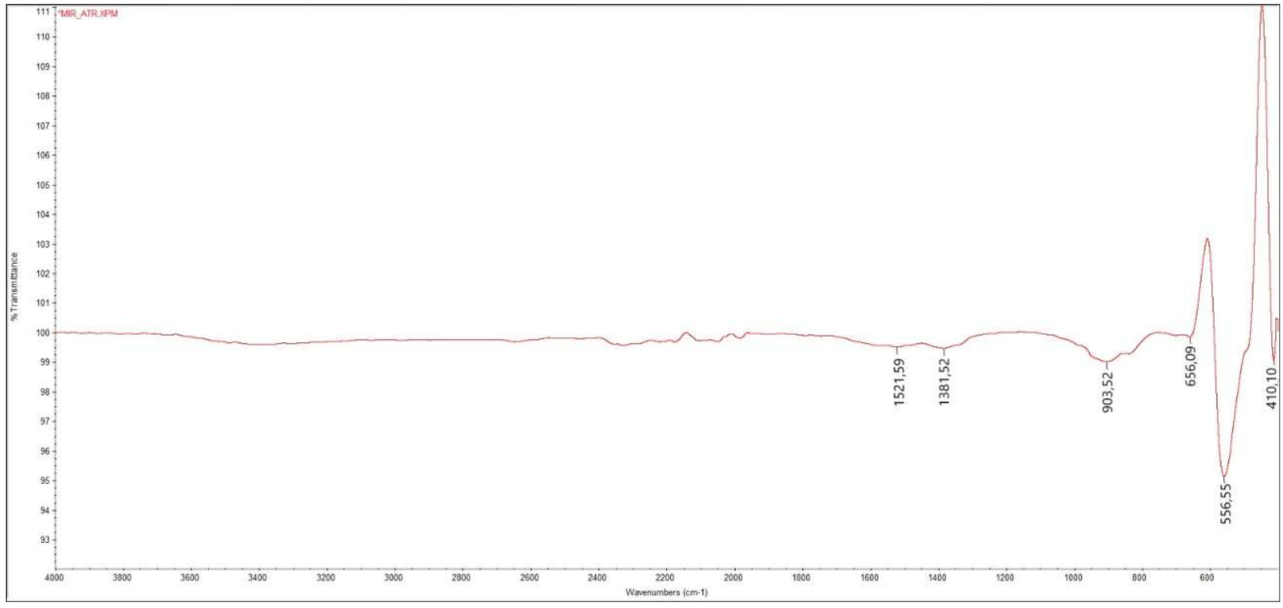


Figure 5. FTIR spectrum of *C. sinensis*-mediated zinc oxide nanoflowers. (Peaks corresponding to Zn–O bond vibrations (400–1000 cm^{-1}) and surface-bound phytochemical carboxylate groups (~1381 and ~1521 cm^{-1}) are indicated.).

mL at 72 h. These findings confirm that prolonged exposure enhances the inhibitory effects of ZnO nanoparticles on L929 cell viability.

Expression analysis of interleukin-1 beta (IL-1β) and interleukin-10 (IL-10)

Following treatment of L929 cells with the non-toxic concentration of biosynthesized ZnO NPs, both IL-1β and IL-10 exhibited dynamic expression changes over time.

For IL-1β, the 24-hour group demonstrated a clear increase in expression (Mean = 1.257, 95% CI: 0.913–1.601) compared to the control group (Mean = 1.014, 95% CI: 0.840–1.188). At 48 h, IL-1β expression decreased (Mean = 0.979, 95% CI: 0.815–1.143), and this reduction persisted at 72 h (Mean = 1.034, 95% CI: 0.838–1.231), indicating a time-dependent decline following the initial upregulation. The analysis revealed a statistically significant difference in IL-1β expression ($F(3,8) = 5.50$, $p = 0.024$) between treatment groups, with a large effect size ($\eta^2 = 0.67$). Post-hoc comparisons using Tukey's multiple comparison test demonstrated that the 24-hour treatment resulted in significantly higher values compared with the control, 48-, and 72-hour groups ($p < 0.05$

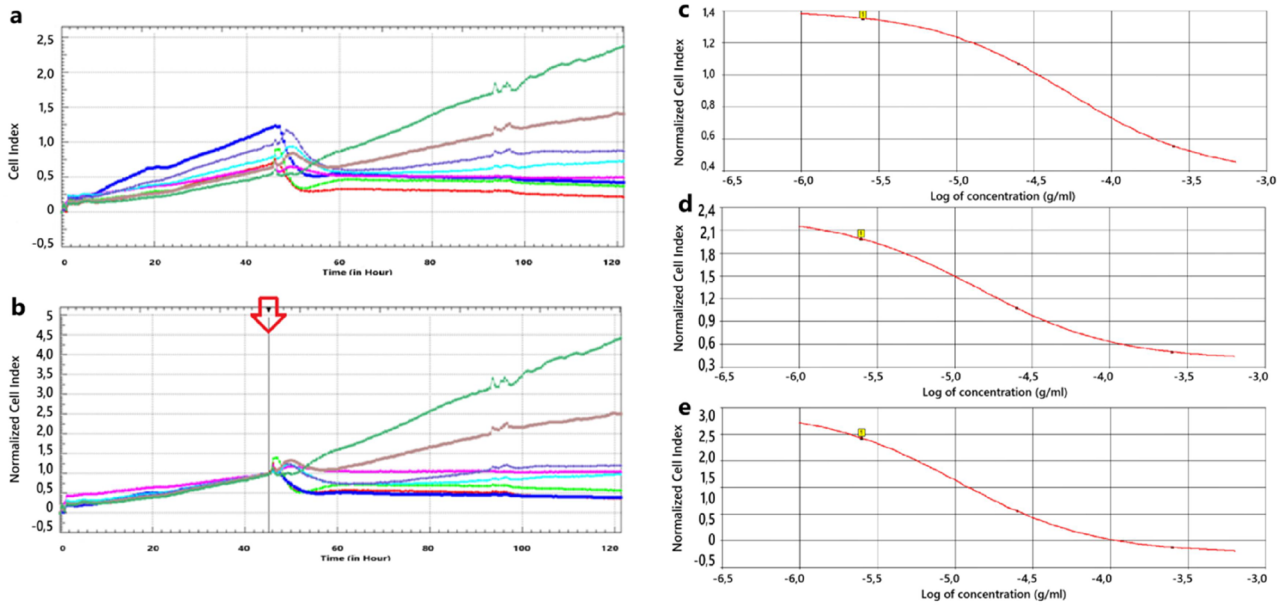


Figure 6. Real-time monitoring of L929 cytotoxicity and dose–response modelling following zinc oxide nanoparticle exposure. (a) CI over time. (b) NCI over time. The red arrow denotes the time of ZnO nanoparticle addition, marking the onset of the acute response phase. (c) Sigmoidal dose–response curve after 24 h exposure (IC_{50} = 52.3 µg/mL). (d) Sigmoidal dose–response curve after 48 h exposure (IC_{50} = 14.1 µg/mL). (e) Sigmoidal dose–response curve after 72 h exposure (IC_{50} = 10.5 µg/mL).

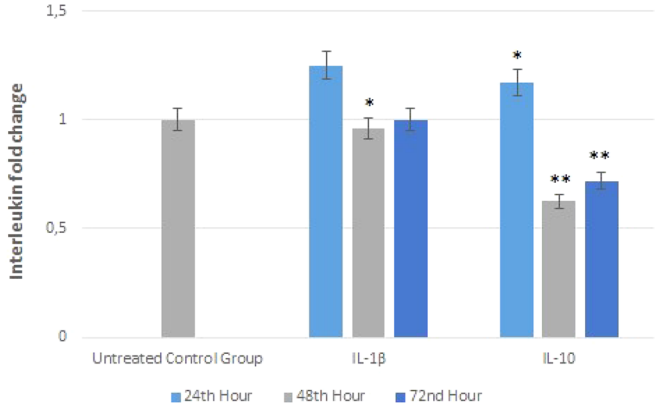


Figure 7. Expression levels of IL-1β and IL-10 in L929 fibroblasts following treatment with *C. sinensis*-mediated ZnO nanoparticles (2.5 µg/mL) at 24-, 48-, and 72-hours post-treatment, quantified by ELISA. Statistical analysis was performed using one-way ANOVA followed by Tukey's post-hoc test. *(*p < 0.05, **p < 0.01)*.

for all). No statistically significant differences were observed among the control, 48-, and 72-hour groups.

Similarly, IL-10 expression peaked at 24 h (Mean = 1.158, 95% CI: 1.134–1.182), relative to the control group (Mean = 1.006, 95% CI: 0.965–1.047). However, a substantial downregulation was detected at later time points, with expression declining to 0.634 at 48 h (95% CI: 0.562–0.706) and partially recovering to 0.853 at 72 h (95% CI: 0.839–0.868). The differences among experimental groups analysis revealed a highly significant effect of treatment on the measured IL-10 expression ($F(3,8) = 483.64$, $p < 0.0001$), with an extremely large effect size ($\eta^2 = 0.995$). Post-hoc analysis using Tukey's multiple comparison test demonstrated that all treatment groups differed significantly from one another ($p < 0.05$).

Overall, both cytokines showed a significant early induction at 24 h ($p = 0.025$) followed by a progressive reduction at 48 and 72 h, suggesting an acute but transient activation of inflammatory and anti-inflammatory pathways after ZnO NP exposure (Figure 7).

Bax, bcl-2, and p53 gene regulation

Relative quantification of Bax, Bcl-2, and p53 mRNA expression in L929 cells following treatment with *C. sinensis*-mediated ZnO nanoparticles at a non-toxic concentration revealed time-dependent modulation of apoptotic gene expression (Figures 8 and 9).

Group-wise analysis demonstrated significant temporal effects on apoptotic regulators. Bax expression showed a marked increase at 24 and 48 h compared to control ($p < 0.01$, $\eta^2 = 0.85$), indicating enhanced pro-apoptotic signalling. In contrast, Bcl-2 expression was significantly reduced at 48 h ($p < 0.05$, $\eta^2 = 0.78$), while no significant changes were observed at 24 or 72 h. Similarly, p53 expression peaked at 48th h, exhibiting a significant increase relative to control ($p < 0.05$, $\eta^2 = 0.71$), followed by a decline at 72 h. Collectively, these findings indicate maximal pro-apoptotic modulation at 48 h post-treatment.

At 24th h, Bax expression increased to 3.20-fold (95% CI: 0.008–131.5), and p53 expression rose to 1.86-fold (95% CI: 0.89–3.89) relative to control. Although point estimates suggested upregulation, the wide confidence interval for Bax—likely reflecting technical variability and low expression levels—limited definitive interpretation at this time point. Bcl-2 expression showed a modest, non-significant increase to 1.08-fold (95% CI: 0.74–1.56).

By 48 h, Bax expression further increased to 3.34-fold (95% CI: 0.86–12.9). While the confidence interval overlapped unity, statistical analysis confirmed a significant increase relative to control ($p < 0.05$). p53 expression also increased to 2.98-fold (95% CI: 0.65–13.6). Concurrently, Bcl-2 expression decreased

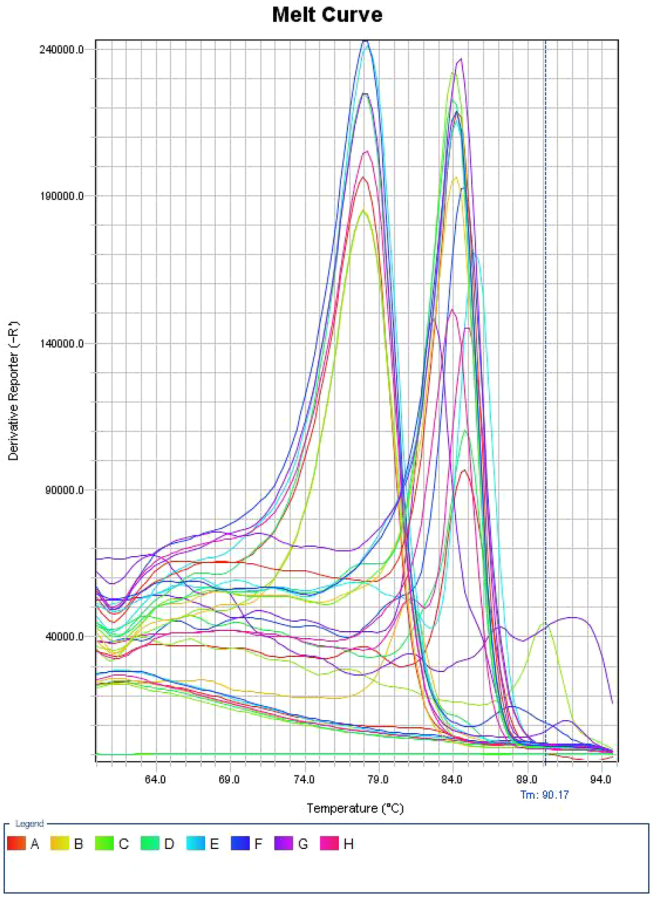


Figure 8. qPCR melting curve profiles of Bcl-2, Bax, and p53 transcripts in treated and control groups. The plate includes control samples (p53, bcl2, bax, gapdh), experimental groups (24, 48, 72), and no-template controls (NTCs). Gene targets are arranged in columns: p53 (col. 1), Bcl2 (col. 2), Bax (col. 3), gapdh (col. 4), with replicates across rows. Wells A4, B5, C5, and D5 are NTCs.

to 0.39-fold (95% CI: 0.06–2.39), although this reduction did not reach statistical significance.

At 72nd h, Bax expression returned to near-baseline levels (1.06-fold, 95% CI: 0.003–371), whereas p53 expression remained elevated at 2.08-fold (95% CI: 0.83–5.24). Bcl-2 expression exhibited a slight increase to 1.16-fold (95% CI: 0.003–510), again with wide confidence intervals indicating substantial measurement variability.

The Bax/Bcl-2 ratio, a key indicator of apoptotic susceptibility, increased substantially at 48th h, driven primarily by Bax upregulation and concomitant reduction in Bcl-2 expression, supporting enhanced apoptotic potential during this treatment period.

Discussion

C. sinensis extract was employed to synthesise flower-shaped ZnO NPs exhibiting a characteristic yellowish-white appearance. FESEM images confirmed the critical role of *C. sinensis* extract as a shape-directing agent during the biosynthesis, facilitating the formation of nanoflower morphologies. This unique architecture is increasingly being leveraged for targeted biomedical applications. Notably, peony-shaped ZnO nanoflowers have recently demonstrated significant dual

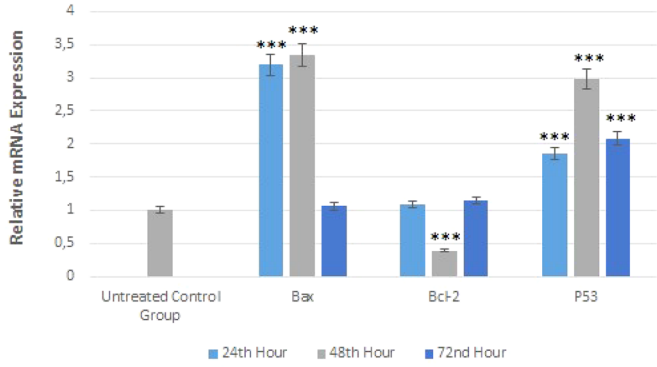


Figure 9. Relative gene expression of *Camellia sinensis* biofabricated zinc oxide nanoparticles on L929 cells for Bax, Bcl-2 and p53 genes at 24th, 48th and 72nd hours. Statistical analysis was performed using one-way ANOVA followed by Tukey's post-hoc test (*$p < 0.05$, **$p < 0.01$, ***$p < 0.001$).

anticancer and anti-amyloid activity, showing high biocompatibility in normal cells and fibroblasts while inducing dose-dependent cytotoxicity in cancer cell lines (Girigoswami et al. 2024). This underscores the potential of morphologically controlled ZnO nanostructures, such as those synthesised in this study, to elicit selective biological responses, a principle central to their development as engineered xenobiotic-like agents for therapy.

Bioactive phytochemicals in plant extracts, such as polyphenols and flavonoids, play a crucial role in nanoparticle nucleation, growth, and morphology control at elevated alkaline pH, as supported by the current results and previous reports (Sattar et al. 2023). This proposed role of phytochemicals as capping agents is directly supported by our FTIR spectroscopic data, which confirms the coordination of organic carboxylate groups from the extract to the ZnO surface. This interaction is critical for directing the nanoflower morphology and passivating the surface, thereby modulating the nanoparticle's interfacial behaviour and its xenobiotic-like profile in biological systems.

DLS and zeta potential analyses provided comprehensive physicochemical characterisation of *C. sinensis*-mediated ZnO NPs, integral to understanding their colloidal stability, surface charge, and size distribution—all essential determinants of xenobiotic behaviour and biological performance. The mean hydrodynamic diameter of ~259 nm represents the effective size of the *C. sinensis*-capped ZnO nanoflower complexes in aqueous suspension, which includes the contribution of the stabilising phytochemical corona and the hydration layer. This value is larger than the nanoscale dimensions of the individual flower petals observed in dry-state FESEM images (Figure 2), a characteristic feature of biogenically synthesised, hierarchically structured nanoparticles. This discrepancy confirms the successful functionalization of the ZnO nanostructures with organic molecules from the plant extract, contributing to their high colloidal stability as evidenced by the zeta potential (~32.35 mV). The combination of a relatively uniform hydrodynamic size (SD: 26.0 nm) with a narrow size distribution indicates the synthesis of stable NPs within the upper nanoscale range, which is advantageous in reducing cellular toxicity by minimising aggressive membrane penetration and modulating controlled Zn^{2+} ion release (Ates et al.

2013; Naqvi et al. 2019; Babayevska et al. 2022; Mitjans et al. 2023). Monodispersity, affirmed by a single sharp peak in size distribution, facilitates predictable biodistribution and consistent interactions with biological interfaces. Transmission intensity measurements confirmed the optical clarity of the suspension, implying minimal aggregation or impurity presence, a feature critical for reducing nanoparticle-related xenobiotic stress and unpredictable toxic effects.

Zeta potential measurements further reinforce the colloidal stability of ZnO NPs, where a value below −30 mV denotes strong electrostatic repulsion among particles, effectively preventing aggregation in biological media (Honary and Zahir 2013). This stability not only improves nanoparticle dispersion but also influences biodistribution and interaction with plasma proteins, potentially mitigating xenobiotic accumulation and cytotoxicity *in vivo*. Electrophoretic mobility data corroborated the zeta potential results, suggesting that the biosynthesized ZnO nanoflowers possess favourable physicochemical properties for sustained biological activity with minimised cytotoxicity. The presence of this organic corona was further confirmed by Fourier-transform infra-red (FTIR) spectroscopy. The spectrum displayed characteristic Zn–O stretching vibrations (< 1000 cm^{-1}) alongside distinct peaks corresponding to carboxylate groups (~1381 and ~1521 cm^{-1}), providing direct evidence of phytochemicals from *C. sinensis* extract bound to the nanoparticle surface. This biomolecular capping layer is integral to the observed colloidal stability and is a key determinant of the subsequent biological interactions.

Cytotoxicity assays revealed a time- and dose-dependent decrease in CI, mirroring prior reports on ZnO NPs' cytotoxic effects. Notably, the IC_{50} values indicate moderate toxicity, higher than some comparable studies yet consistent with others, potentially attributable to the larger particle size and surface coating from biomolecules in *C. sinensis* extract, which may moderate Zn^{2+} release and reduce reactive oxygen species (ROS) generation (AlSalhi et al. 2020; Wadekar et al. 2025). Prolonged exposure (up to 72 h) heightened cytotoxic effects, underscoring the importance of evaluating extended exposures relevant to xenobiotic accumulation and chronic toxicity (Şeker et al. 2014).

Inflammatory cytokine profiling illustrated a biphasic response in L929 mouse fibroblasts following ZnO NP treatment at sub-toxic concentrations. Early upregulation of pro-inflammatory IL-1β alongside anti-inflammatory IL-10 after 24 h suggests activation of cellular defence mechanisms, attempting to balance inflammation and tissue repair amid nanoparticle-induced oxidative or mechanical stress (Zhai et al. 1997; Sahu et al. 2014; Senapati et al. 2015). With extended exposure to 48–72 h, cytokine expression declined, likely reflecting compromised cellular viability confirmed by cytotoxicity data. This cytokine pattern reflects a dynamic xenobiotic response where initial inflammatory signalling is followed by immune exhaustion or cell death, important considerations for evaluating the safety and long-term impact of ZnO NPs in biomedical and environmental contexts.

At the molecular level, apoptotic pathway analysis showed time-dependent modulation of key regulatory genes Bax, Bcl-2, and p53, revealing intricate cellular responses to *C. sinensis*-derived ZnO nanoflowers. A significant early increase in pro-apoptotic Bax and tumour suppressor p53 transcripts at 24 h indicates mitochondrial-mediated apoptosis initiation, consistent with stress-induced DNA damage responses and nanoparticle-triggered ROS production documented in xenobiotic literature (Wilhelmi et al. 2013; Wang et al. 2021). The slight rise in anti-apoptotic Bcl-2 may represent a transient cellular attempt to counterbalance apoptosis, but later data showed a shift favouring apoptosis with increased Bax and p53 and decreased Bcl-2 expression at 48 h. At 72 h, reduced expression of Bax and p53 alongside resurging Bcl-2 levels suggests selective survival of resistant cell populations or cellular adaptation mechanisms aiming at restoring homeostasis (Wang et al. 2021). This dynamic regulation of apoptotic signalling highlights the complex cellular interplay in response to nanoparticle exposure and indicates a potential synergistic pro-apoptotic effect mediated by bioactive components capping the ZnO nanoflowers.

Overall, the study demonstrates that green synthesis of ZnO nanoflowers using *C. sinensis* extract is an effective, scalable, and eco-friendly approach yielding NPs with favourable physicochemical characteristics and moderate biocompatibility. The biomolecule-mediated synthesis not only influences nanoparticle morphology and stability but also modulates xenobiotic properties, including reduced cytotoxicity and dynamic inflammatory and apoptotic cellular responses. This approach decreases exposure to toxic chemicals common in traditional synthesis and aligns with green chemistry principles, potentially mitigating environmental and health-related xenobiotic risks.

However, several limitations must be acknowledged. Although the use of L929 mouse fibroblasts provides a standardised and relevant model for initial nanosafety assessment, it inherently restricts the broader interpretation of the xenobiotic and apoptotic responses observed. Different cell types—including epithelial barriers, immune cells, and stem cells—possess distinct uptake mechanisms, metabolic capacities, and stress-response pathways, which may yield markedly different sensitivity, IC_{50} values, cytokine modulation patterns, and gene-expression profiles following ZnO nanoflower exposure. Thus, the findings derived from murine fibroblasts cannot be directly extrapolated to human tissues or cancerous cells without further validation. In addition, *in vitro* assays do not fully recapitulate the systemic complexity, biodistribution, or nanoparticle metabolism characteristic of *in vivo* environments. Furthermore, while untreated cells served as the essential baseline, the cytokine and gene expression assays did not include classical pharmacological positive controls (e.g. LPS for inflammation, staurosporine for apoptosis). Their inclusion in future studies would provide a valuable benchmark for comparing the relative potency of the nanoparticle-induced stress response. The specific phytochemicals responsible for nanoparticle reduction, capping, and bioactivity were not isolated or quantified, leaving mechanistic insights incomplete and contributing to potential variability in reproducibility. Long-term colloidal stability, aggregation under physiological conditions, and storage-related alterations also remain unexplored, despite their critical influence on xenobiotic behaviour and clinical

translation of ZnO nanoflowers. Future studies integrating comprehensive phytochemical profiling, diverse cellular models, and *in vivo* xenobiotic toxicology will be essential for strengthening mechanistic understanding and ensuring the safe application of green-synthesised ZnO nanostructures. Moreover, despite the absence of X-ray diffraction (XRD) analysis due to technical constraints, which precludes definitive confirmation of the crystalline phase and crystallite size of the synthesised nanostructures, the collective evidence from UV-Vis spectroscopy (characteristic ZnO band-gap absorption), FTIR analysis (Zn–O and carboxylate bonding), FESEM morphology, and the calcination-based synthesis protocol strongly supports the successful formation of ZnO nanoparticles with surface functionalization by *C. sinensis* phytochemicals.

In conclusion, this study demonstrates a reproducible green approach for fabricating *C. sinensis*-mediated ZnO nanoflowers that exhibit physicochemical stability and moderate cytotoxicity. The nanoparticles triggered transient apoptotic and inflammatory signalling consistent with xenobiotic-like stress adaptation in mammalian fibroblasts. These results suggest that bio-engineered ZnO nanostructures can interact with cellular defence mechanisms in a controlled manner, providing insights into the biological fate and toxicokinetic behaviour of engineered nanomaterials. Future studies should extend these observations to different cell types and *in vivo* models to define dose-response relationships and metabolism pathways more precisely.

Acknowledgements

Special thanks are extended to Assoc. Prof. Dr. Meliha Koldemir Gündüz (Kutahya Health Sciences University) for generously sharing her expertise, time, and access to the cell culture laboratory during the in vitro studies; Asst. Prof. Dr. Fatma Ebru Koç (Istanbul Gelisim University) for her valuable insights into the green synthesis of ZnO NPs and; Asst. Prof. Dr. Abbas Ali Husseini (Istanbul Gelisim University) for his valuable insights in the molecular genetic experiments and assessments.

Ethics approval and consent to participate

Not applicable.

Consent for publication

Not applicable.

Authors' contributions

SYB: Conceptualization, Methodology, Formal analysis, Writing, Reviewing, and Editing. All authors have read and approved the manuscript.

Disclosure statement

The authors have no conflict of interest to declare.

Funding

This study did not receive specific research funding.

ORCID

Serap Yesilkir Baydar http://orcid.org/0000-0001-6311-4302

Data availability statement

The data that support the findings of this study are available from the corresponding author upon reasonable request.

References

Ali SG et al. 2022. Green synthesis of silver nanoparticles from *Camellia sinensis* and its antimicrobial and antibiofilm effect against clinical isolates. Materials. 15(19):6978. https://doi.org/10.3390/ma15196978

AlSalhi MS et al. 2020. Therapeutic potential assessment of green synthesized Zinc Oxide nanoparticles derived from fennel seeds extract. Int J Nanomedicine. 15:8045–8057. https://doi.org/10.2147/IJN.S272734

Ates M, Daniels J, Arslan Z, Farah IO, Rivera HF. 2013. Comparative evaluation of impact of Zn and ZnO nanoparticles on brine shrimp (Artemia salina) larvae: effects of particle size and solubility on toxicity. Environ Sci Process Impacts. 15(1):225–233. https://doi.org/10.1039/c2em30540b

Atmaca H, Bozkurt E, Kısım A, Uslu R. 2016. Comparative analysis of XTT assay and xCELLigence system by measuring cytotoxicity of resveratrol in human cancer cell lines. Turkish J Biochem. 41(6):413–421. https://doi.org/10.1515/tjb-2016-0128

Babayevska N et al. 2022. ZnO size and shape effect on antibacterial activity and cytotoxicity profile. Sci Rep. 12(1):8148. https://doi.org/10.1038/s41598-022-12134-3

Baskaran N, Subash A. 2021. Green synthesis and characterization of Zinc Oxide nanoparticles (ZnO NPs) from *Camellia sinensis* leaf extract and its potential of antibacterial activity and acetyl cholinesterase inhibitory activities. JPRI. 33(51A):134–147. https://doi.org/10.9734/jpri/2021/v33i51A33477

Baydar SY, Çağlar TA, Koç FE. 2025. Biosynthesis of Zinc Oxide Nanoparticles Using Dried Leaves of *Camellia sinensis*: methods to Characterize and Assess Their Effects on Mesenchymal Stem Cell Viability. Springer US; p. 1–13.

Benaiche G, Belhaddad OE, Djaidja S, Mechegueg L. 2025. Eco-friendly synthesis of Zinc Oxide nanoparticles using *Camellia sinensis* leaf extracts. Asian J Green Chem. 9(2):220–230.

Bibi I et al. 2017. Nickel nanoparticle synthesis using *Camellia sinensis* as reducing and capping agent: growth mechanism and photo-catalytic activity evaluation. Int J Biol Macromol. 103:783–790. eng. https://doi.org/10.1016/j.ijbiomac.2017.05.023

Dhanya R, Suganthi KS, Rajan KS. 2014. Studies on scale-up of synthesis of ZnO nanoparticles. Asian J Chem. 26(14):4273–4276. https://doi.org/10.14233/ajchem.2014.16100

Droepenu EK, Wee BS, Chin SF, Kok KY, Maligan MF. 2022. Zinc Oxide nanoparticles synthesis methods and its effect on morphology: a review.

Eric Kwabena D et al. 2021. Zinc Oxide nanoparticles synthesis methods and its effect on morphology: a review. Biointerface Res Appl Chem. 12:4261–4292.

Girigoswami A et al. 2024. Peony-shaped Zinc Oxide nanoflower synthesized via hydrothermal route exhibits promising anticancer and anti-amyloid activity. BMC Pharmacol Toxicol. 25(1):101. https://doi.org/10.1186/s40360-024-00830-x

Hamed R, Obeid RZ, Abu-Huwaij R. 2023. Plant mediated-green synthesis of Zinc Oxide nanoparticles: an insight into biomedical applications. Nanotechnol Rev. 12(1):20230112. https://doi.org/10.1515/ntrev-2023-0112

Hassan A, Elebeedy D, Matar ER, Fahmy Mohamed Elsayed A, Abd El Maksoud AI. 2021. Investigation of angiogenesis and wound healing potential mechanisms of Zinc Oxide nanorods. Front Pharmacol. 12:661217. https://doi.org/10.3389/fphar.2021.661217

Honary S, Zahir F. 2013. Effect of zeta potential on the properties of nano-drug delivery systems - a review (part 1). Trop J Pharm Res. 12(2):255–264. https://doi.org/10.4314/tjpr.v12i2.19

Hussien NA, Khalil M, Schagerl M, Ali SS. 2025. Green synthesis of Zinc Oxide nanoparticles as a promising nanomedicine approach for anti-cancer, antibacterial, and anti-inflammatory therapies. Int J Nanomedicine. 20:4299–4317. eng. https://doi.org/10.2147/IJN.S507214

Ibrahim AMH et al. 2021. The effect of surface modification of TiMg composite on the in-vitro degradation response, cell survival, adhesion, and proliferation. Mater Sci Eng C Mater Biol Appl. 127:112259. https://doi.org/10.1016/j.msec.2021.112259

Jiang J, Pi J, Cai J. 2018. The advancing of Zinc Oxide nanoparticles for biomedical applications. Bioinorg Chem Appl. 2018:1062562–1062518. https://doi.org/10.1155/2018/1062562

Karamanlioglu M, Yesilkir-Baydar S. 2022. Production and characterization of a coconut oil incorporated gelatin-based film and its potential biomedical application. Biomed Mater. 17(4):045014. https://doi.org/10.1088/1748-605X/ac6c67

Kumar MN et al. 2023. Eco-friendly synthesis of Zinc Oxide nanoparticles using *Camellia sinensis* (green tea) and its characterization. IJPSS. 35(20):56–61. https://doi.org/10.9734/ijpss/2023/v35i203785

Lee J et al. 2008. The control of cell adhesion and viability by Zinc Oxide nanorods. Biomaterials. 29(27):3743–3749. https://doi.org/10.1016/j.biomaterials.2008.05.029

Limame R et al. 2012. Comparative analysis of dynamic cell viability, migration and invasion assessments by novel real-time technology and classic endpoint assays. PLoS One. 7(10):e46536. https://doi.org/10.1371/journal.pone.0046536

Mahajan M et al. 2025. Green synthesis of ZnO nanoparticles using Justicia adhatoda for photocatalytic degradation of malachite green and reduction of 4-nitrophenol. RSC Adv. 15(4):2958–2980. https://doi.org/10.1039/d4ra08632e

Mahamuni PP et al. 2019. Synthesis and characterization of Zinc Oxide nanoparticles by using polyol chemistry for their antimicrobial and antibiofilm activity. Biochem Biophys Rep. 17:71–80. https://doi.org/10.1016/j.bbrep.2018.11.007

Mahdi Ismail SM, Ahmed SM, Abdulrahman AF, AlMessiere MA. 2023. Characterization of green synthesized of ZnO nanoparticles by using pinus brutia leaves extracts. J Mol Struct. 1280:135063. https://doi.org/10.1016/j.molstruc.2023.135063

Mitjans M et al. 2023. Size matters? A comprehensive in vitro study of the impact of particle size on the toxicity of ZnO. Nanomaterials. 13(11):1800. https://doi.org/10.3390/nano13111800

Murali M et al. 2023. Zinc Oxide nanoparticles prepared through microbial mediated synthesis for therapeutic applications: a possible alternative for plants [Review. Front Microbiol. 14:1227951. https://doi.org/10.3389/fmicb.2023.1227951

Naiel B, Fawzy M, Halmy MWA, Mahmoud AED. 2022. Green synthesis of Zinc Oxide nanoparticles using Sea Lavender (Limonium pruinosum L. Chaz.) extract: characterization, evaluation of anti-skin cancer, antimicrobial and antioxidant potentials. Sci Rep. 12(1):20370. https://doi.org/10.1038/s41598-022-24805-2

Naqvi QU et al. 2019. Size-dependent inhibition of bacterial growth by chemically engineered spherical ZnO nanoparticles. J Biol Phys. 45(2):147–159. https://doi.org/10.1007/s10867-019-9520-4

Narayana A et al. 2020. Green and low-cost synthesis of Zinc Oxide nanoparticles and their application in transistor-based carbon monoxide sensing. RSC Adv. 10(23):13532–13542. https://doi.org/10.1039/d0ra00478b

Popa ML, Preda MD, Neacşu IA, Grumezescu AM, Ginghină O. 2023. Traditional vs. microfluidic synthesis of ZnO nanoparticles. Int J Mol Sci. 24(3):1875. https://doi.org/10.3390/ijms24031875

Sahu D, M KG, Vijayaraghavan R. 2014. Size-dependent effect of Zinc Oxide on toxicity and inflammatory potential of human monocytes. J Toxicol Environ Health A. 77(4):177–191. https://doi.org/10.1080/15287394.2013.853224

Sattar R et al. 2023. Biogenic synthesis of Zinc Oxide nanoparticles using leaves extract of *Camellia sinensis* for photocatalytic and biological applications. J Optoelectr Biomed Mater. 15:1–9.

Şeker Ş, Elçin AE, Yumak T, Sınağ A, Elçin YM. 2014. In vitro cytotoxicity of hydrothermally synthesized ZnO nanoparticles on human periodontal ligament fibroblast and mouse dermal fibroblast cells. Toxicol in Vitro. 28(8):1349–1358. https://doi.org/10.1016/j.tiv.2014.06.016

Senapati VA, Kumar A, Gupta GS, Pandey AK, Dhawan A. 2015. ZnO nanoparticles induced inflammatory response and genotoxicity in human blood cells: a mechanistic approach. Food Chem Toxicol. 85:61–70. https://doi.org/10.1016/j.fct.2015.06.018

Senthilkumar SR, Thirumal S. 2014. Green tea (*Camellia sinensis*) mediated synthesis of Zinc Oxide (ZnO) nanoparticles and studies on their antimicrobial activities. Int J Pharm Pharm Sci. 6:461–465.

Shalahuddin F, Almekahdinah S, Nandiyanto A. 2019. Preliminary economic study on the production of ZnO nanoparticles using a sol-gel synthesis method. JKimTerapIndones. 21(1):1–6. https://doi.org/10.14203/jkti.v21i1.407

Słota D et al. 2021. Preparation, characterization, and biocompatibility assessment of polymer-ceramic composites loaded with salvia officinalis extract. Materials (Basel). 14(20):6000. https://doi.org/10.3390/ma14206000

Wadekar S, Hate M, Chaughule R. 2025. Biosynthesis of Zinc Oxide nanoparticles and their cytotoxicity study on fibroblast cell line using MTT assay. Orient J Chem. 41(2):409–417. https://doi.org/10.13005/ojc/410209

Wang J et al. 2021. The role of apoptosis pathway in the cytotoxicity induced by fresh and aged Zinc Oxide nanoparticles. Nanoscale Res Lett. 16(1):129. https://doi.org/10.1186/s11671-021-03587-y

Wiesmann N, Tremel W, Brieger J. 2020. Zinc Oxide nanoparticles for therapeutic purposes in cancer medicine. J Mater Chem B. 8(23):4973–4989. https://doi.org/10.1039/d0tb00739k

Wilhelmi V et al. 2013. Zinc Oxide nanoparticles induce necrosis and apoptosis in macrophages in a p47phox- and Nrf2-independent manner. PLoS One. 8(6):e65704. https://doi.org/10.1371/journal.pone.0065704

Wu F, Harper BJ, Harper SL. 2019. Comparative dissolution, uptake, and toxicity of Zinc Oxide particles in individual aquatic species and mixed populations. Environ Toxicol Chem. 38(3):591–602. https://doi.org/10.1002/etc.4349

Zhai Q-H, Futrell N, Chen F-J. 1997. Gene expression of IL-10 in relationship to TNF-α, IL-1β and IL-2 in the rat brain following middle cerebral artery occlusion. J Neurol Sci. 152(2):119–124. https://doi.org/10.1016/s0022-510x(97)00154-8